

Article

Results of ^{147}Sm – ^{143}Nd (ID-TIMS) and U–Pb (SHRIMP-II) Dating of Rocks and Minerals of the Chromite-Bearing Kluchevskoy Ophiolite Massif (the Eastern Segment of the Urals) and Their Geological Interpretation

Vladimir N. Smirnov, Kirill S. Ivanov, Yuriy L. Ronkin  and Yuriy V. Erokhin * 

The Zavaritsky Institute of Geology and Geochemistry of the Ural Branch of the Russian Academy of Sciences, Akademika Vonsovskogo Str. 15, 620110 Yekaterinburg, Russia

* Correspondence: erokhin-yu@yandex.ru; Tel.: +7-(950)-194-2752

Abstract: The Urals is one of the reference mobile belts of the mafic type characterized by a wide development of ophiolites which are associated with numerous deposits of chromites of significant industrial importance. In this regard, the estimation of the age of the rocks of the ophiolite association will be useful for analyzing the regularities of the formation of chromite deposits. This work presented the results of age dating of the rocks of the chromite-bearing Kluchevskoy mafic–ultramafic massif, one of the most representative of all the ophiolite-type massifs in the Urals, by two isotopic methods. The U–Pb (SHRIMP-II, VSEGEI) dating of the zircon dominated assemblage from rocks of different composition of both crustal and mantle sections of the Kluchevskoy ophiolite massif yielded similar dates ranging from 456 to 441 Ma. The study of the composition of silicate inclusions in zircon grains of this assemblage showed that they are represented by typical metamorphic minerals: low-*T* amphibole, albite, and an epidote-group mineral. The *P*–*T* conditions of zircon crystallization established via the examination of the composition of minerals in these inclusions showed that the crystallization of the predominant fraction of zircons coincides in time with the lower epidote–amphibolite and upper green-schist facies metamorphism of rocks happening under the decompression conditions, i.e., during their exhumation from the deep crustal level (8–13 km). A small amount of zircons of late generation showed a wide spread in age (277.4–318.1 Ma). The time of their crystallization corresponds to the stage of metamorphism associated with the collision orogeny in the Ural mobile belt. The more ancient ^{147}Sm – ^{143}Nd age of 514 Ma should be assumed as the formation time of the rocks (or its upper age boundary).



Citation: Smirnov, V.N.; Ivanov, K.S.; Ronkin, Y.L.; Erokhin, Y.V. Results of ^{147}Sm – ^{143}Nd (ID-TIMS) and U–Pb (SHRIMP-II) Dating of Rocks and Minerals of the Chromite-Bearing Kluchevskoy Ophiolite Massif (the Eastern Segment of the Urals) and Their Geological Interpretation. *Minerals* **2022**, *12*, 1369. <https://doi.org/10.3390/min12111369>

Academic Editors: Mauro C. Geraldes and Ramiro Matos

Received: 15 September 2022

Accepted: 25 October 2022

Published: 27 October 2022

Publisher's Note: MDPI stays neutral with regard to jurisdictional claims in published maps and institutional affiliations.



Copyright: © 2022 by the authors. Licensee MDPI, Basel, Switzerland. This article is an open access article distributed under the terms and conditions of the Creative Commons Attribution (CC BY) license (<https://creativecommons.org/licenses/by/4.0/>).

Keywords: Urals; ophiolites; U–Pb; ^{147}Sm – ^{143}Nd dating

1. Introduction

The Urals is one of the reference mobile belts of the mafic type characterized by a wide development of ophiolites which are associated with numerous deposits of chromites of significant industrial importance. In this regard, the estimation of the age of the rocks of the ophiolite association will be useful for analyzing the regularities of the formation of chromite deposits. The numerous isotopic ages of rocks of ophiolite associations have been obtained over the past two decades [1–10]. Nevertheless, at present the problem of the correct dating of the formation of these rocks cannot be completely resolved. The isotopic ages of the rocks of the ophiolite complexes of the Urals cover a very wide age range from the Paleoproterozoic to the middle of the Silurian (2800–428 Ma). Since most zircon ages obtained are off the Neoproterozoic (Vendian) and the Early Silurian, it was suggested that the Vendian (Neoproterozoic) and Silurian stages of the ophiolite formation could be distinguished on the eastern slope of the Urals [5]. Later on, the age heterogeneity of mantle peridotite ophiolites indicating the complex evolution of the mantle section of the

ophiolite complexes of the Urals throughout the Proterozoic was revealed (refs. [4,8,11], etc.) and a range of the Paleozoic age data (from Early Ordovician to middle of the Silurian (480–428.5 Ma ago) was clarified ([3,4,10,11], etc.). There is no widely accepted interpretation of the age data obtained and an assessment of the degree of their validity. When discussing the most ancient ages (2.8–1.9 Ga and older) obtained by different isotopic methods (Sm–Nd and Re–Os for the whole rock and U–Pb for zircon), all researchers agree that they reflect the processes of evolution of mantle matter, since they significantly exceed the time of formation of the Urals mobile belt. However, there is no consensus on the geological meaning of Neoproterozoic (0.6–0.5 Ga) and Paleozoic (480–428.5 Ma) ages. Some geologists consider a distinct age limit of 600–500 Ma ago as the time of the beginning of the formation of the oceanic crust [5,6], while others believe that it is one of the stages of mantle transformation [4,8]. In addition, numerous Paleozoic age data are associated both with the formation time of the ophiolite association [3,5,7] and with one of the stages of transformation of rocks of the ophiolite association [4,11].

This work aimed at studying the Kluchevskoy mafic–ultramafic massif in order to obtain new age data and establish the formation time of chromite-bearing rocks of the ophiolite association of the Urals. This research included the U–Pb (SIMS) zircon dating of rocks of the Kluchevskoy massif and the ^{147}Sm – ^{143}Nd isotopic investigations, as well as the study of the crystallization conditions of dated zircon grains.

2. Analytical Methods

The chemical compositions of rocks and minerals were examined in the Institute of Geology and Geochemistry of the Ural Branch of the Russian Academy of Sciences (Yekaterinburg, Russia). The content of the main petrogenic elements was estimated by the X-ray fluorescence method using a CPM-18 spectrometer; the concentrations of Na_2O , FeO , and LOI were measured by the chemical method. Detection limits (wt%) for SiO_2 are 1–100, TiO_2 —0.01–10, Al_2O_3 —0.30, Fe_2O_3 —0.5–20, FeO —0.35–90, MnO —0.1–2.0, MgO —0.3–50, CaO —0.3–40, Na_2O —0.2–20, P_2O_5 —0.05–5.0, and LOI—0.0001–50. Accuracy of analysis is 4.2%–5.2% for SiO_2 , 22% for TiO_2 , 11%–20% for Al_2O_3 , 14%–19% for Fe_2O_3 , 12% for MnO , 7%–11% for MgO , 7%–18% for CaO , 0.2%–2.0% for Na_2O , and 0.01% for LOI.

The content of trace elements was measured by the ICP-MS method on an ELAN-9000 mass spectrometer after acid decomposition (a mixture of hydrofluoric and nitric acids, ratio 5:1) of geological material in a Multiwave 3000 microwave oven with XQ80 rotor (cell material: quartz). All analytical procedures were performed in a clean room using ultrapure reagents. Typical operating conditions of the mass spectrometer ELAN 9000 for multi-element analysis of samples are as follows: RF Power 1175 W; Nebulizer Gas Flow 0.8 L/min; Argon Gas Pressure 60 psi; Lens Voltage 7.25 V; Analog Stage Voltage –2078 V; Pulse Stage Voltage 1300 V; Discriminator Threshold 300; AC Rod Offset –9.5; Detector Mode Dual; Sweeps/reading 30; Rinse/Flush Delay Time 34 s; Read Delay Time 14 s. The ranges of detection limits for elements (ppm) were determined for Cs, Sr, Ba, V, Y, La, Ce, Pr, Nd, Sm, Eu, Gd, Tb, Dy, Ho, Er, Tm, Yb, Lu, Zr, Hf, Nb, Ta, Sn, Pb, Tl, Bi, Sb, Mo, W, U, Th 0.1–1 ppm, for Li, Rb, Be, Sc, Cr, Co, Ni, Cu, Ga, Ge, Cd, Te, Sn 1–10 ppm and for K 10–100 ppm. The quality control of the obtained results was carried out via a simultaneous analysis of internal reference samples and rock samples, the concentration of elements in which is certified with accuracy close to 1% rel., and the procedure of acid separation provisions did not raise any doubts about its accuracy (we used samples SG-1A, SGD-1A, and BCR-2). Simultaneous statistics measurements of verification samples and standard samples of rocks made it possible to assess the quality of the analysis of the entire series of geological samples (reproducibility results of simultaneous analysis of standard samples is the most reliable estimate of the accuracy of the analysis of geological samples and, depending on the element and its concentration, did not exceed 3%–10% rel.).

The compositions of minerals inclusions in zircon grains were measured using a CAMECA SX 100 electron probe microanalyzer. Standards: Mg, Ca, Si—diopside; Na, Al—albite; Fe—almandine; Cr—chrome-diopside; K—orthoclase; Mn—rhodonite; Ti— TiO_2 .

Detection limits (wt%) were Si—0.03, Ti—0.05, Al—0.02, Cr—0.08, Fe—0.09, Mn—0.08, Mg—0.02, Ca—0.03, Na—0.03, and K—0.02.

Sm and Nd concentrations and $^{147}\text{Sm}/^{144}\text{Nd}$, $^{143}\text{Nd}/^{144}\text{Nd}$ ratios were measured via isotope dilution (ID) mass spectrometry using a $^{149}\text{Sm}+^{150}\text{Nd}$ mixed spike and subsequent analysis using a Triton multicollector thermal ionization mass spectrometer (TIMS) in static mode. The correct implementation of the isotope dilution thermal ionization mass spectrometry (ID-TIMS) was carried out via a preliminary measurement of Sm and Nd contents by the HR/ICP-MS method and the subsequent optimization of isotopic dilution parameters. A more detailed description of analytical procedures is provided in ref. [12]. The control over the accuracy and reproducibility of the concentrations of Sm (6.535 ± 0.032 , MSWD = 1.4), Nd (28.55 ± 0.17 , MSWD = 1.6), and $^{147}\text{Sm}/^{144}\text{Nd}$ (0.13820 ± 0.00024 , MSWD = 1.07), $^{143}\text{Nd}/^{144}\text{Nd}$ (0.512638 ± 0.000009 , MSWD = 0.97) atomic ratios was executed via the analysis the BCR-2 (n = 24) and La Jolla (0.511856 ± 0.000005 , MSWD = 0.67, n = 51) standards, respectively.

The zircon grains were extracted from samples weighing from 120 kg (mantle dunite) to 60 kg (gabbro) using a common set of methods, including crushing the sample to a fraction <0.315 mm, washing the crushed material to a gray concentrate, magnetic separation, separation in heavy liquids, and manual selection of zircon grains under binoculars. The analysis of the U–Pb isotope systematics of zircons was performed using a high-resolution ion microprobe (SHRIMP-II) (VSEGEL, Center of Isotope Research, St. Petersburg, Russia) in accordance with the methodology described in [13,14]. Temora and 91500 standards were used as a reference [15–18], for which, according to the average ratios $^{206}\text{Pb}/^{238}\text{U}$, 416.26 ± 8.06 Ma, MSWD = 1.4, n = 47; 1059 ± 21 Ma, MSWD = 1.8, n = 53, respectively, were obtained.

3. Geological Settings

The Kluchevskoy massif is located in the Eastern zone of the Middle Urals, which is composed of Paleozoic volcanogenic, volcanogenic–sedimentary, and sedimentary strata enclosing blocks, lenses, and sheets of rocks of the ophiolite association, as well as numerous intrusions varying in composition and age. As a rule, there are thick strata (or their tectonic fragments) of sodium basalts at the base of the volcanogenic sections of the eastern sector of the Urals and most often aphyric tholeiitic basalts containing rare layers of red jasper (radiolarites). These strata correspond to the upper part of the oceanic type of crust and demonstrate a Middle-Late Ordovician age in the research area, which was confirmed by the discovery of conodonts in jaspers. Andesites, their tuffs, abundant volcanomictic sandstones, and limestones gradually appear above this section among the Silurian and Devonian basalts, where porphyry structures are characteristic of volcanites. It indicates the formation of the upper parts of volcanogenic sections in island-arc conditions. This indicated that the Ordovician tholeiitic basalts of this part of the Urals were not formed in open ocean conditions, but most likely have a back-arc nature. The Eastern zone of the Middle Urals extends along the eastern margin of the Urals mobile belt [19]. To the east, the Paleozoic complexes of this zone go under the sedimentary cover of the West Siberian Plate (see for more details ref. [20]). On the west side they are separated from the structures of the open part of the Urals by a system of faults, the Bazhenovo suture zone [21].

At the level of erosion, the Kluchevskoy massif represents a drop-shaped structure (Figure 1), which extends submeridionally for about 25 km, reaching a maximum width of 7.5 km in the south. The exposed area is about 85 km². According to geophysical data the thickness of the massif increases sharply from 0.8 km in the northern part to 5–6 km in the southern one. All contacts with the host rocks are tectonic, steeply dipping at an angle of 50–80°. The eastern and southern contacts dip beneath the massif, whereas the northern and western ones dip in the opposite direction. Two recognizable rock complexes are well distinguished in the structure of the massif: dunite–harzburgite (metamorphic mantle peridotites [22]) and dunite–wehrlite–clinopyroxenite–gabbro (cumulative ophiolite complex [22]). The rocks of the dunite–harzburgite complex dominate,

almost entirely composing the northern and central parts of the massif (Figure 1). The contact with the dunite–wehrlite–clinopyroxenite–gabbro complex is tectonic. As evidenced from geophysical data, the contact surface gently dips at an angle of 30–40° beneath dunites and harzburgites. Thus, the latter forms a nappe sheet overlying the rocks of the dunite–wehrlite–clinopyroxenite complex.

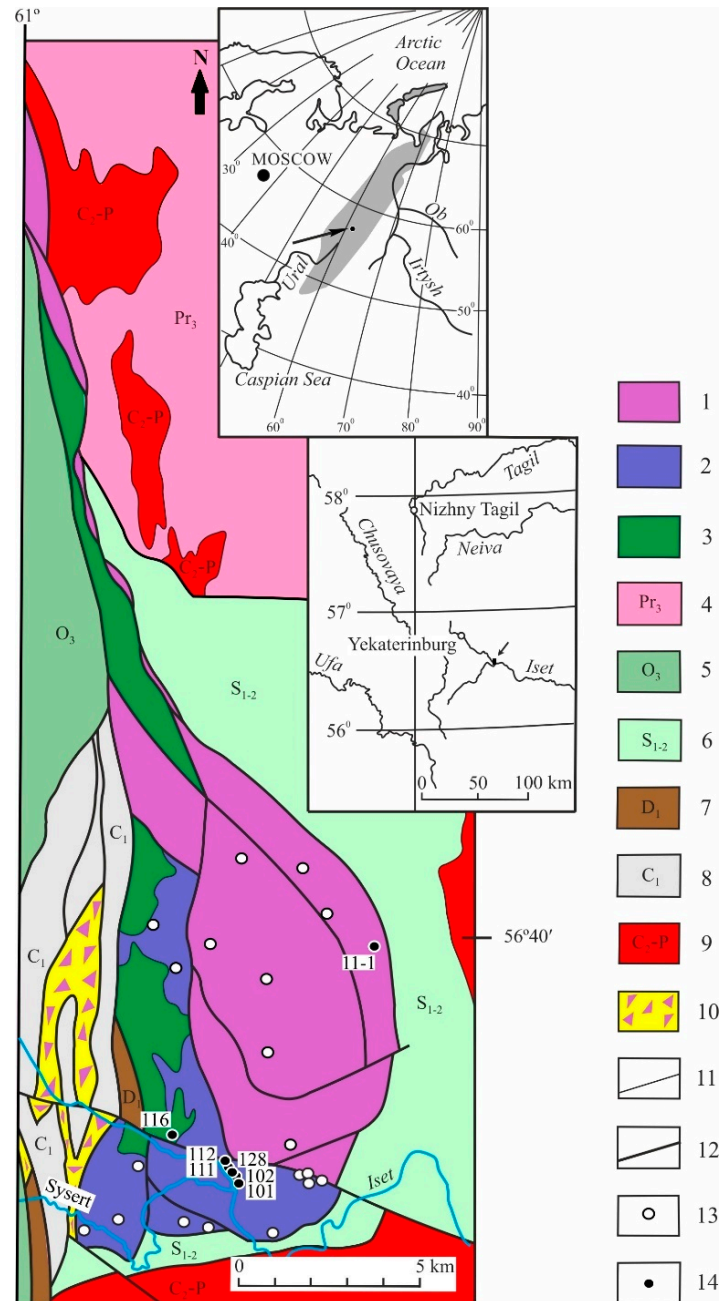


Figure 1. Geological scheme of the Kluchevskoy ophiolite massif with sampling sites for isotopic analysis. (1) Harzburgite complex (mantle ultramafic rocks), (2) layered strata of dunites and clinopyroxenites (crustal part of the ophiolite section), (3) gabbro of the layered (crustal) part of the ophiolite section. Rocks of the frame: (4) Neoproterozoic gneisses, amphibolites, and crystalline schists; (5) Late Ordovician dunite volcano-sedimentary rocks; (6) Silurian terrigenous-carbonate strata; (7) Early Devonian limestones; (8) Early Carboniferous terrigenous strata; (9) Late Paleozoic granitoids; (10) polymictic serpentinite mélange; (11) undisturbed geological boundaries; (12) faults; (13) deposits and occurrences of chromite ores; (14) sampling sites for isotope dating.

The dunite–harzburgite complex. The dunite–harzburgite complex, composing the most part of the massif, is poorly exposed. Due to this fact, mainly core rock samples from a few wells were studied. The dunite–harzburgite complex represents alternation of dunites and harzburgites with gradual transitions between them. It should be noted that there is an extremely irregular distribution of orthopyroxene in rocks, from 25%–30% to 0%. The dunite zones range from a few centimeters to several meters, sometimes reaching the first tens of meters. They are diverse in shape, from isometric and lenticular schliers to quickly wedging bands and echeloned bands replacing each other, as well as bodies of complex irregular shape. The complex irregular shape of the areas composed of dunites and harzburgites is the main feature of this association of rocks. The proportion of dunites in the total rock volume varies quite widely, averaging about 25%. The harzburgite zones separating the dunite bodies are from 1 to 15 m wide, usually 1–6 m. Dunites and, to a much lesser extent, harzburgites of this complex contain bodies of massive, rarely nodular, and disseminated chromite ores. Ore zones form pockets, stocks, or short lenses up to 100 m long and a length-to-thickness ratio of approximately 1:10. The northern half of the Klyuchevskoy massif is characterized by the presence of lenses, bands, and zones composed of epigenetic dunites. The epigenetic origin of dunites is established based on sharp contacts with harzburgites and numerous apophyses. The formation of this variety of dunites most likely is the final phase of the transformation (recrystallization) of the mantle substance. The proportion of these dunites is from 30% to 100%, averaging about 40% of the total volume of rocks. The thickness of epigenetic dunite bodies ranges from a few meters to several hundred meters.

The metamorphic processes (several stages of serpentinization) are manifested irregularly in the rocks of this complex. They led to the formation of lizardite, lizardite–antigorite, and antigorite serpentinites, as well as partial serpentinization of dunites and harzburgites. Zones of chrysolitization and hydrothermal transformations of rocks, expressed in the formation of talc, carbonate, and less often chlorite, are associated with low-amplitude fault zones with a dip at a high angle formed at the late stages of the development of the region (collisional and post-collisional). As a rule, a degree of serpentinization is at least 70%. The near-contact zones where the serpentinization processes were most intense are up to 1 km wide extend along the western and eastern margins of the massif. They are composed of completely recrystallized antigorite serpentinites, which are missing any signs of primary rocks. The chrysolitization and hydrothermal alteration of rocks led to the formation of talc, carbonate, and less often chlorite, and were confined to the fault zones. Antigorite serpentinites enclose the zones of olivine–antigorite rocks, which are the products of higher-*T* metamorphism.

All rocks of the dunite–harzburgite complex show distinct signs of intense tectonic transformation. S.A. Shcherbakov [23] distinguished three stages of high-*T* plastic deformations, which, in his opinion, occurred partly at the mantle and crustal levels. Later they were replaced by brittle deformations developed within a thin local fracture zone simultaneously with serpentinization or after it.

The dunite–wehrlite–clinopyroxenite–gabbro complex. The dunite–wehrlite–clinopyroxenite–gabbro complex composes several tectonic blocks in the southern and western parts of the Kluchevskoy massif (Figure 1). Dunites, wehrlites, and clinopyroxenites compose a WE-trending tectonic block in the southern part of the massif. There are also small clinopyroxenite bodies in the western part, to the north of the above-mentioned block. The rocks of the southern block are distinctly layered. The lower part of the section, represented by dunites serpentinized to varying degrees enclosing bodies of syngenetic impregnated, rarely massive chromite ores, crops out in the southeastern part of the block. Ore bodies are mainly NW-dipping at an angle of 50–80°, following the structure of this part of the ophiolite association. Higher in the section, there is a macro-rhythmic banded succession of dunites, wehrlites, and olivine clinopyroxenites with the gradual disappearance of the first two rock varieties in the upper part, which is entirely composed of clinopyroxenites, which are recognizable in the exposures. The study of the composition of melt inclusions in the

chrome spinelides grains from ore bodies revealed that basalts with a low alkali content ($\text{Na}_2\text{O} + \text{K}_2\text{O}$ up to 1.06 wt%) and an increased Ca content (up to 18 wt%) were probably initial melts for the layered series [24]. The most complete section of the Kluchevskoy ophiolite complex is traced along the Sysert River, for a distance of 1.5 km upstream from its confluence with the Iset River and along the latter for 2 km upstream from the mouth of the Sysert River.

Gabbroids comprise three relatively small bodies elongated in a submeridional direction along the western margin of the massif.

A degree of serpentinization of dunites usually ranges from 60% to 80%. The ratio between early loop-shaped serpentine and later antigorite varies noticeably. Metamorphic transformations of the least altered dunite varieties are limited by the development of early loop-shaped serpentinization at extremely insignificant development of antigorite veins. However, rocks containing loop-shaped serpentine and antigorite in comparable quantities dominate. Accessory chromite is partially replaced by chrome-magnetite. Antigorite serpentinites, which are completely missing any signs of the primary rocks, are developed as a contact zone along the southern margin of the massif. Talc–carbonate, serpentine–chlorite–talc rocks, as well as talc-rich rocks form a thin contact zone between ultramafic and host rocks. They are less common inside the massif being confined to tectonic zones. Antigoritization is developed in olivine clinopyroxenites of the southwestern part of the massif; the proportion of antigorite sometimes reaches 20%–30%.

Gabbros are different than other rocks of the layered part of the ophiolite section as they possess a higher degree of transformations. They preserved no primary mineral composition and are represented by highly deformed gabbro and apo–gabbro greenschists, in which the grains of the primary dark-colored mineral are replaced by an aggregate of low temperature fibrous amphibole (uralite), and the plagioclase is completely saussuritized. The high degree of gabbro deformations is explained by the location of these rocks inside and in close proximity to a large fault, the Bazhenovo suture, the formation of which was connected with the collision stage of the evolution of the Ural mobile belt.

S.A. Shcherbakov [23] distinguished three generations of folds in the rocks of this complex corresponding to three stages of high-*T* plastic deformations. In his opinion, they cannot be considered as analogs of deformations in the dunite–harzburgite complex. It can be only said that the last stages of the observed deformations deformed both rock associations in their close to modern position, which led to the formation of conformal arched folds with subvertical bends. The magmatic stratification of the dunite–wehrlite–clinopyroxenite–gabbro complex was not disturbed during these deformations.

A peculiar feature of the dunite–wehrlite–clinopyroxenite–gabbro complex is the absence of orthopyroxene-bearing rocks in its composition. The orthopyroxene is a typical mineral of rocks of the layered section of most ophiolite complexes. Based on this feature, it is partially similar to a certain degree to the dunite–wehrlite–clinopyroxenite–gabbro complex of the Kluchevskoy massif with banded mafic–ultramafic series of the Ural Platinum Belt. However, the geochemical features clearly indicate the ophiolitic origin of the Kluchevskoy massif.

Geochemical features of rocks. The main features of rocks of the dunite–harzburgite complex are high Mg#, higher Cr and Ni contents, and low contents of CaO, Al_2O_3 , TiO_2 , and lithophilic rare elements (Table 1). Rocks of the dunite–wehrlite–clinopyroxenite–gabbro complex are characterized by high Mg# and higher contents of refractory siderophilic elements (Cr, Ni). At this, they are depleted in low-melting siderophilic elements (Ti, V) and lithophilic elements (Rb, Sr), rare earths, with a predominance of HREE over LREE (Table 1). Compared with similar rocks of massifs of the Ural Platinum Belt, refractory elements (Os, Ir, and Ru) predominate in the platinoids of the studied rocks [25].

Table 1. The content of the main petrogenic elements (wt%) and impurity elements (ppm) in the rocks of the Kluchevskoy massif.

	127	102	103	106	105	113	114	116
SiO ₂	39.10	34.18	34.07	42.10	42.15	51.36	51.04	45.59
TiO ₂	0.03	0.01	0.01	0.04	0.03	0.06	0.06	0.07
Al ₂ O ₃	0.52	0.41	0.40	0.66	0.64	2.04	1.85	17.76
Fe ₂ O ₃	3.30	6.73	6.78	4.06	4.34	3.39	2.37	1.50
FeO	4.33	1.80	1.40	2.10	2.50	1.80	2.50	2.10
MnO	0.09	0.15	0.14	0.15	0.15	0.13	0.13	0.07
MgO	41.05	41.70	41.45	35.34	34.75	21.09	21.80	13.30
CaO	0.50	0.02	-	6.02	6.42	17.72	17.84	14.94
Na ₂ O	0.17	0.31	0.31	0.31	0.31	0.31	0.35	1.10
P ₂ O ₅	0.05	-	-	-	-	0.01	-	-
LOI	11.12	14.30	16.00	9.50	8.80	2.20	2.20	3.10
Sum	100.30	99.62	100.56	100.28	100.09	100.11	100.14	99.50
Mg/(Fe + Mg)	0.91	0.90	0.91	0.91	0.91	0.89	0.89	0.87
Li	0.256	0.291	0.357	2.686	2.507	3.299	8.966	12.086
K	9.7	13.1	22.7	19.6	15.2	34.3	54.3	15.7
Rb	0.066	0.052	0.79	0.59	0.104	0.169	0.369	0.428
Cs	0.003	0.003	0.009	0.016	0.013	0.026	0.068	0.044
Be	0.005	0.008	0.034	0.002	0.009	0.012	0.009	0.031
Sr	-	0.36	3.39	3.29	3.33	4.99	5.53	147
Ba	3.74	0.77	0.18	1.37	1.76	1.56	4.41	7.22
Sc	5.52	3.22	9.47	30.18	35.50	61.84	59.87	18.12
V	17.8	11.9	22.4	53.5	59.8	172.3	163.7	58.9
Cr	2451	3179	4667	1050	1056	1714	2785	1167
Co	100	106	297	78.5	82.2	41.4	42.9	28.9
Ni	1323	1104	2036	642	649	182	206	257
Y	0.090	0.059	0.097	0.573	0.637	1.539	1.754	2.227
La	0.029	0.025	0.077	0.017	0.027	0.038	0.068	0.193
Ce	0.055	0.057	0.135	0.060	0.080	0.135	0.216	0.591
Pr	0.005	0.007	0.012	0.013	0.014	0.027	0.040	0.095
Nd	0.027	0.031	0.049	0.095	0.096	0.185	0.271	0.543
Sm	0.005	0.005	0.010	0.051	0.058	0.102	0.135	0.210
Eu	0.003	0.001	0.001	0.021	0.021	0.049	0.054	0.142
Gd	0.007	0.008	0.014	0.091	0.099	0.198	0.244	0.313
Tb	0.001	0.001	0.002	0.017	0.018	0.037	0.045	0.057
Dy	0.013	0.011	0.019	0.115	0.127	0.297	0.346	0.389
Ho	0.003	0.002	0.004	0.023	0.027	0.067	0.078	0.082
Er	0.016	0.007	0.012	0.066	0.076	0.189	0.226	0.239
Tm	0.003	0.001	0.002	0.010	0.011	0.026	0.032	0.037
Yb	0.025	0.010	0.017	0.061	0.071	0.173	0.213	0.230
Lu	0.004	0.002	0.003	0.009	0.010	0.027	0.031	0.034
Zr	-	0.260	0.478	0.247	0.264	0.651	0.893	1.861
Hf	-	0.006	0.016	0.010	0.015	0.032	0.045	0.071
Nb	0.001	0.030	0.054	0.016	0.054	0.010	0.015	0.033
Ta	0.002	0.003	0.029	0.028	0.006	0.006	0.006	0.007
Zn	41.7	31.8	73.5	32.1	37.0	12.7	17.3	14.9
Pb	0.784	-	-	0.204	0.081	-	-	0.191
Cu	7.213	16.445	48.395	6.893	9.133	10.604	37.805	48.835
Ga	0.455	0.283	0.589	0.540	0.615	1.772	1.726	9.144
Tl	0.009	0.227	0.332	0.038	0.068	0.042	0.087	0.021
Ge	0.717	0.560	1.498	1.017	1.074	1.598	1.538	0.822
Cd	0.021	-	0.028	0.037	0.061	0.029	0.048	0.024

Table 1. Cont.

	127	102	103	106	105	113	114	116
Bi	0.003	0.001	0.022	0.005	0.006	-	0.007	0.009
Sb	4.546	0.037	0.070	0.206	0.245	0.279	0.156	0.268
Te	0.079	0.034	0.118	0.007	0.027	0.024	0.028	0.003
Sn	0.014	0.009	0.017	0.061	0.045	0.031	0.008	0.075
Mo	0.176	0.313	0.508	0.119	0.157	0.006	0.008	0.081
W	6.961	1.197	0.814	0.065	0.162	0.141	0.300	0.065
U	0.080	0.005	0.011	-	0.002	0.004	0.009	0.012
Th	0.003	0.006	0.014	0.005	0.006	0.006	0.013	0.025

Notes: 127—serpentinized dunite of the dunite–harzburgite complex. Rocks of the dunite–wehrlite–clinopyroxenite–gabbro complex: 102, 103—serpentinized dunites; 106, 105—serpentinized wehrlites; 113, 114—olivine clinopyroxenites; 116—sossuritized gabbro.

Chromite mineralization of the Kluchevskoy massif. To date, 19 small deposits and ore occurrences of chromites have been identified within the Kluchevskoy massif [26]. Seven of them are localized in the northern (mantle) part (dunite–harzburgite complex) and twelve deposits and ore occurrences are confined to the lower part (dunites) of the stratified part of the section (dunite–wehrlite–clinopyroxenite–gabbro complex). All occurrences of chromites located in the rocks of the dunite–harzburgite complex belong to the magnesian type. Three occurrences are composed of high-chromium ores and four—alumina ores. Deposits and occurrences of chromites in the southern (crustal) part of massif are represented by high-chromium ores of increased ferruginousness.

4. Results

4.1. U–Pb (SIMS) Dating of Zircon Grains

Characteristics of the studied samples. In the course of our research, we dated zircons from four samples: dunite from the mantle peridotite complex, as well as dunite, olivine clinopyroxenite, and gabbro from the crustal (cumulative) part of the ophiolite section. The results of the U–Pb zircon isotope dating are presented in Table 2.

Table 2. U–Pb SHRIMP-II zircon data for the Kluchevskoy massif.

Spot	$^{206}\text{Pb}_c$, %	Concentration, ppm			$\frac{^{232}\text{Th}}{^{238}\text{U}}$	Age, Ma $\frac{^{206}\text{Pb}}{^{238}\text{U}}$	Isotope Ratios ⁽¹⁾				Rho	D, %
		U	Th	$^{206}\text{Pb}^*$			$\frac{^{207}\text{Pb}^*}{^{235}\text{U}}$	±%	$\frac{^{206}\text{Pb}^*}{^{238}\text{U}}$	±%		
Zircon from dunite 11-1, early generation												
1.1	0	44	14	2.57	0.326	422 ± 10	0.524	5.9	0.0676	2.5	0.424	8.5
2.1	2.78	136	102	8.58	0.778	444 ± 9.8	0.533	18	0.0713	2.3	0.128	−17
3.1	1.97	109	55	7.09	0.522	462 ± 11	0.539	16	0.0743	2.4	0.150	−48
5.1	0	48	21	2.82	0.45	426 ± 10	0.547	5.6	0.0683	2.5	0.446	20
6.1	0	41	21	2.62	0.541	464 ± 11	0.562	5.8	0.0747	2.6	0.448	−18
7.1	0.54	98	101	5.9	1.071	436.8 ± 9.4	0.511	7.5	0.0701	2.2	0.293	−35
8.1	0.37	142	93	9.14	0.677	460 ± 9.5	0.56	5.5	0.0748	2.1	0.382	−21
9.1	0.62	112	74	7.12	0.687	457.2 ± 9.8	0.57	7.3	0.0735	2.2	0.301	1.1
Zircon from dunite 11-1, late generation												
1.2	0.71	469	1	18.9	0.003	292.9 ± 5.7	0.338	5.3	0.04649	2	7.6	7.6
2.2	0.11	896	16	34.9	0.018	285.7 ± 5.5	0.3282	2.7	0.04532	2	7.3	7.3
4.1	0.3	585	2	24.5	0.003	305.4 ± 5.9	0.342	3.5	0.04851	2	−24	−24
6.2	1.82	462	16	19.5	0.035	303.8 ± 6.1	0.345	7.5	0.04826	2	−9.0	−9.0
8.2	0.1	957	11	41.6	0.012	318.1 ± 6	0.3716	2.7	0.05059	1.9	6.6	6.6
9.2#	0.27	665	24	25.2	0.037	277.4 ± 5.4	0.312	3.4	0.04397	2	−6.0	−6.0

Table 2. Cont.

Spot	$^{206}\text{Pb}_c$, %	Concentration, ppm			$\frac{^{232}\text{Th}}{^{238}\text{U}}$	Age, Ma $^{206}\text{Pb}/^{238}\text{U}$	Isotope Ratios ⁽¹⁾				Rho	D, %
		U	Th	$^{206}\text{Pb}^*$			$\frac{^{207}\text{Pb}^*}{^{235}\text{U}}$	$\pm\%$	$\frac{^{206}\text{Pb}^*}{^{238}\text{U}}$	$\pm\%$		
Zircon from dunite 101												
1.1	0.00	453	669	29	1.53	462 ± 8.3	0.596	3.2	0.0743	1.9	0.594	14
2.1	0.00	265	194	15.4	0.76	422.3 ± 7.8	0.520	2.9	0.0677	1.9	0.655	4.2
3.1	0.00	109	81	6.65	0.76	441 ± 8.8	0.578	5.1	0.0708	2.1	0.412	23
4.1	0.14	304	283	18.4	0.96	439.8 ± 8	0.539	3.7	0.0706	1.9	0.514	−2.9
4.2	0.00	82	46	5.14	0.57	452.4 ± 9.8	0.552	4.7	0.0727	2.2	0.468	−9.0
5.1	0.00	34	11	2.02	0.34	430.1 ± 10	0.514	5.8	0.069	2.5	0.431	−16
6.1	0.00	64	23	3.92	0.37	443.4 ± 9.4	0.528	4.4	0.0712	2.2	0.500	−22
7.1	0.18	857	1061	53.2	1.28	448.2 ± 7.8	0.553	2.4	0.072	1.8	0.750	−1.7
7.2	0.00	79	29	4.89	0.38	451.2 ± 9.3	0.545	4.1	0.0725	2.1	0.512	−15
8.1	0.00	48	16	3.04	0.35	459.6 ± 11	0.558	5.5	0.0739	2.4	0.436	−14
9.1	0.00	238	154	14	0.67	427.7 ± 7.8	0.515	2.8	0.0686	1.9	0.679	−10
10.1	0.00	127	75	7.58	0.61	431.9 ± 8.8	0.536	3.6	0.0693	2.1	0.583	5.3
Zircon from olivine pyroxenite 128												
1.1#	0	57	50	14	0.9	1610 ± 29	4.16	2.6	0.2837	2.0	0.769	7.4
1.2#	0.1	212	199	54.6	0.97	1693 ± 29	4.359	2.2	0.3004	1.9	0.864	1.5
2.1	0	97	40	6.03	0.42	450.6 ± 9.3	0.54	4.1	0.0724	2.1	0.512	−20
3.1	0	286	346	18.2	1.25	459.9 ± 7.9	0.578	2.3	0.0739	1.8	0.783	4.4
4.1#	0	266	235	15.2	0.91	413.2 ± 7.4	0.507	2.7	0.0662	1.8	0.667	4.8
5.1	0	92	79	5.83	0.89	458.4 ± 9.6	0.563	4.2	0.0737	2.2	0.524	−7.0
6.1	0.89	61	33	3.79	0.56	449 ± 11	0.525	10	0.0722	2.4	0.240	−42
7.1#	0	314	284	18.6	0.93	429.5 ± 7.9	0.523	2.7	0.0689	1.9	0.704	−3.7
7.2#	0.25	856	7	32.3	0.01	276.5 ± 5	0.3157	3.0	0.04382	1.8	0.600	6.7
8.1	0	129	110	7.95	0.88	447 ± 9	0.563	3.7	0.0718	2.1	0.568	8.1
9.1	0	67	48	4.2	0.73	454 ± 10	0.574	4.9	0.073	2.3	0.469	7.8
10.1#	0	173	166	9.98	1	419 ± 8	0.505	3.5	0.0672	2.0	0.571	−7.0
Zircon from gabbro 116												
1.1	1.51	66	11	4.19	0.17	452 ± 10	0.526	15	0.0727	2.3	0.153	−48
2.1	2.56	39	4	2.51	0.1	457 ± 12	0.690	23	0.0735	2.8	0.122	48
3.1	0.05	488	60	30.4	0.13	452 ± 7	0.569	2.8	0.0726	1.6	0.571	6.9
4.1	0.52	189	30	12.1	0.16	460 ± 8	0.555	4.8	0.0739	1.7	0.354	−18
5.1	3.87	50	10	3.33	0.2	461 ± 13	0.580	30	0.0742	2.9	0.097	3.8
6.1	3.0	93	19	6.03	0.21	453 ± 10	0.590	21	0.0729	2.2	0.105	18
6.2	2.79	70	7	4.62	0.11	464 ± 11	0.710	19	0.0747	2.4	0.126	48
7.1	2.02	101	8	6.51	0.08	457 ± 9	0.630	17	0.0734	2.1	0.124	33
8.1	2.75	107	21	6.8	0.2	448 ± 9	0.571	17	0.072	2.1	0.124	12
9.1	5.69	54	10	3.69	0.19	467 ± 15	0.600	35	0.0751	3.3	0.094	12

Notes: #—U-Pb SRIMP-II data excluded from the corresponding age calculations; errors $\pm 1\sigma$; Pbc and Pb * denote common and radiogenic lead, respectively; ⁽¹⁾ conventional Pb corrected using measured ^{204}Pb ; D, discordance; Rho is the correlation coefficient.

Sample 11-1 was collected from mantle dunites in a small ballast quarry in the eastern part of the massif (56°39.538' N, 061°09.827' E). Dunites are characterized by a high degree of serpentinization (80%–90%). The predominant serpentine mineral is antigorite; lizardite is less common. Serpentinization of rocks is manifested irregularly. The completely ser-

pentinized dunites enclose weakly serpentinized 3–8 mm sites, consisting mainly of relict grains of primary minerals. Mg olivine ($Mg\# = 0.97\text{--}0.98$) is predominant; chromium spinel and single grains of orthopyroxene and clinopyroxene occur in subordinate amounts of 1%–3%.

Description of dated zircons. Ten zircon grains extracted from a 120 kg sample are represented by colorless, transparent, subidiomorphic prismatic crystals or their fragments with an elongation coefficient from 1.25 to 1.4. They are from 150 to 250 μm in length and from 50 to 100 μm across; there are also some fragments of larger crystals. The cathodoluminescent (CL) images (Figure 2a) show that zircon crystals are represented by two generations. Zircon of early generation composes the core of grains, which are usually represented by subidiomorphic short-prismatic crystals with traces of dissolution, sometimes rounded and rarely irregular. The core varies in size from 15×50 to $150 \times 200 \mu\text{m}$; elongation is 1.3–3.3. The zircon of the core has a well-defined rhythmic zoning and, as a rule, sectorial structure. It differs from zircon of the late generation by a low U content in the range of 41–136 ppm (Table 2). The late zircon has no zoning and composes the rims of grains. The U content (462–957 ppm) in rims is noticeably higher than in the core (Table 2).

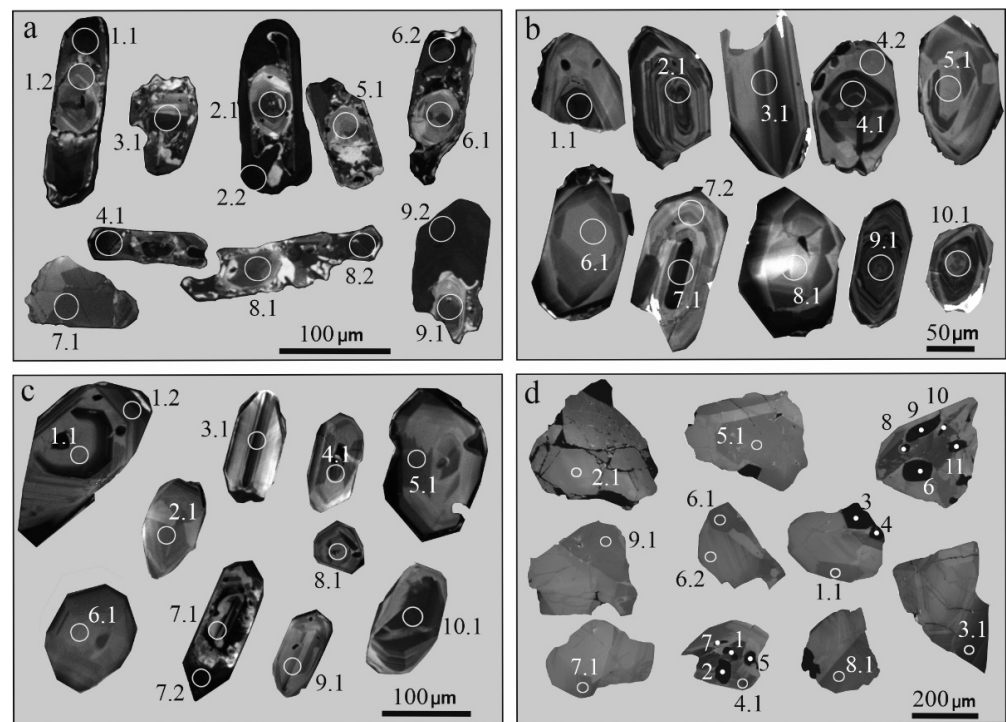


Figure 2. CL images of zircon grains from the Kluchevskoy massif. (a) Zircons from mantle dunite, sample 11-01; (b) zircons from dunite of the layered part of the ophiolite sequence, sample 101; (c) zircons from olivine clinopyroxenite, sample 128; (d) zircons from gabbro, sample 116. The circles show the measurement points of the U-Pb isotope system of zircons. The dots are the points of measurement of the composition of silicate inclusions in zircon grains. The point numbers are the same as in Table 2.

Zircon grains from dunite sample 101 are represented by idiomorphic prismatic crystals (elongation from 1.5 to 2.5) and their fragments varying from 100 to 200 μm along long axis and from 50 to 100 μm across (Figure 2b). All grains show thin rhythmic zoning.

The grains of zircon from olivine clinopyroxenite (sample 128) are morphologically close to the zircon from the dunite of the layered part of the ophiolite (sample 101). They are represented by idiomorphic prismatic zonal crystals (Figure 2c), varying in size from 100 to 200 μm or more along the long axis and from 50 to 110 μm across.

Zircon grains extracted from the gabbro sample 116 are represented by xenomorphic fragments of zonal crystals ranging from 100 to 600 μm in size (Figure 2d). Some grains

have distinct signs of crushing. Sometimes, zircon crystals contain small (35–110 μm) rounded subidiomorphic or elongated inclusions of silicate minerals.

Analytical results. The results of the U–Pb zircon isotope dating are presented in Table 2.

In $^{206}\text{Pb}/^{238}\text{U}$ – $^{207}\text{Pb}/^{235}\text{U}$ concordia diagram (Figure 3a), eight data points of zircons of the early generation form a compact cluster with an age of 446.5 ± 7.1 Ma (Late Ordovician) at $\text{MSWD}_{\text{C+E}} = 1.5$. Zircons of the late generation (six analyses) differed noticeably in age, forming a relatively disconnected cluster localized along the concordia line (277.4–318.1 Ma: the second half of the Carboniferous and the beginning of the Permian). The age calculated from five representative ellipses of this cluster was 300.7 ± 8.8 Ma.

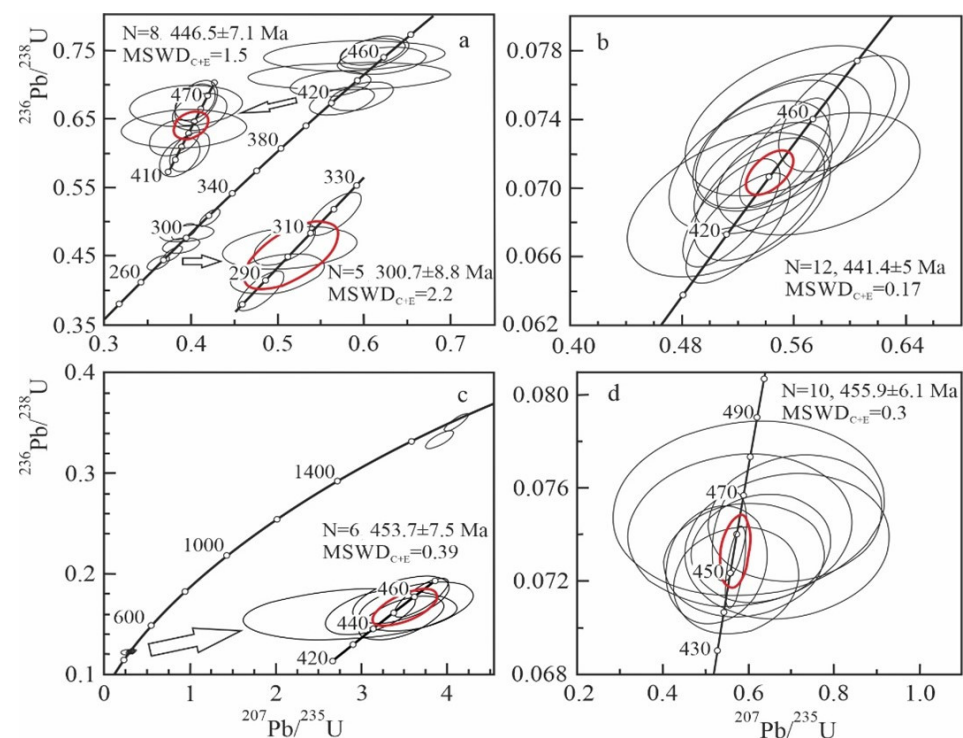


Figure 3. The U–Pb concordia diagrams for zircons from different rock varieties of the Kluchevskoy massif: (a) zircons from mantle dunite, sample 11-01; (b) zircons from dunite of the layered part of the ophiolite sequence, sample 101; (c) zircons from olivine clinopyroxenite, sample 128; (d) zircons from gabbro, sample 116.

Twelve measurements of zircons of dunite sample 101 formed in the Ahrens–Wetherill $^{206}\text{Pb}/^{238}\text{U}$ – $^{207}\text{Pb}/^{235}\text{U}$ isotope diagram (Figure 3b) a cluster with an age of 441.4 ± 5.0 million years at $\text{MSWD}_{\text{C+E}} = 0.17$.

The results of the U–Pb isotope dating of zircon from olivine clinopyroxenite (sample 128) plotted on $^{206}\text{Pb}/^{238}\text{U}$ – $^{207}\text{Pb}/^{235}\text{U}$ concordia diagram (Figure 3c) showed that the analyzed grains were divided into two zircon assemblages significantly different in age. The first one forms a compact cluster ($N = 6$) with a concordant ($\text{MSWD}_{\text{C+E}} = 0.39$) age of 453.7 ± 7.5 Ma. The second one is represented by two points in the age range of 1700–1650 Ma. The occurrence of zircon grains with such ancient ages can most likely be explained by the fact that they were captured by magmatic melt from the mantle protolith.

In the U–Pb isotopic diagram (Figure 3d), ten points of zircons from gabbro of sample 116 were located on the concordia line, forming a cluster that yields the concordant age of 455.9 ± 6.1 Ma at $\text{MSWD}_{\text{C+E}} = 0.3$.

The results of our research showed that most zircon grains in all rock varieties of both the crustal (layered) and mantle parts of the ophiolite association of the Kluchevskoy massif have a close U–Pb age. Its crystallization occurred over a period from 456 to 441 Ma ago,

which corresponds to the Late Ordovician and Llandovery epoch of Silurian according to the present-day International Chronostratigraphic Chart (ver. 2022/02). This means that the U–Pb zircon age data recorded a Late Ordovician–Llandovery event, which is common to all rocks of the ophiolite association without exception.

4.2. Results of ^{147}Sm – ^{143}Nd Dating

In order to perform this analysis, the authors selected a set of rock samples from the layered part of the ophiolite sequence which crops out along the left bank of the Iset River upstream the Sysert River mouth (Figure 1). Sample 102 is serpentinized dunite with a degree of serpentinization of about 60%. The sampling site is the exposure on the left bank of the Iset River, 150 m above its confluence with the Sysert River ($56^{\circ}36.263'$ N, $061^{\circ}06.015'$ E). Sample 111 is a slightly amphibolized clinopyroxenite, collected from the exposure on the left bank of the Iset River, 600 m upstream from its confluence with the Sysert River ($56^{\circ}36.448'$ N, $061^{\circ}05.936'$ E). Sample 112 is a wehrlite containing about 70% clinopyroxene and about 30% serpentinized olivine, which was collected from the exposure on the left bank of the Iset River, 660 m upstream from its confluence with the Sysert River ($56^{\circ}36.481'$ N, $061^{\circ}05.909'$ E). Sample 116 is a green-stone gabbro typical of the ophiolites of the Urals, consisting of a low-temperature amphibole, which completely replaced the primary dark-colored mineral, and a completely sossuritized plagioclase. This sample was collected from the rock exposure on the left bank of the Iset River 2.1 km upstream from its confluence with the Sysert River ($56^{\circ}36.832'$ N and $61^{\circ}04.980'$ E). Along with the whole-rock samples, the monomineral fraction of olivine extracted from dunite and the clinopyroxene monofraction from pyroxenite and wehrlite were used for geochronological studies.

The results of the ^{147}Sm – ^{143}Nd dating of dunite, gabbro, clinopyroxenite, wehrlite, and extracted monofractions of olivine and clinopyroxene are shown in Table 3 and are plotted on the $^{147}\text{Sm}/^{144}\text{Nd}$ – $^{143}\text{Nd}/^{144}\text{Nd}$ evolutionary diagram (Figure 4).

Table 3. ^{147}Sm – ^{143}Nd ID-TIMS data for rocks and minerals of the Kluchevskoy massif.

Numbers of Samples	Rocks, Minerals	Sm (ppm)	Nd (ppm)	$\frac{^{147}\text{Sm}}{^{144}\text{Nd}}$	$\pm 2\sigma$	$\frac{^{143}\text{Nd}}{^{144}\text{Nd}}$	$\pm 2\sigma$
102	dunite	0.0105	0.0753	0.0846	0.0004	0.512574	0.000015
	olivine	0.211	1.34	0.0948	0.0005	0.512612	0.000010
112	wehrlite	0.160	0.296	0.327	0.002	0.513371	0.000021
	clinopyroxene	0.173	0.304	0.344	0.002	0.513462	0.000010
111	clinopyroxenite	0.0568	0.134	0.256	0.001	0.513140	0.000015
	clinopyroxene	0.123	0.294	0.254	0.001	0.513146	0.000015
116	gabbro	0.227	0.694	0.1975	0.0009	0.512950	0.000010

The range of measured $^{147}\text{Sm}/^{144}\text{Nd}$ ratios is rather significant (0.0846 ± 0.0004 – 0.344 ± 0.002). Together with the absence of correlation on the $1/\text{Nd}$ – $^{143}\text{Nd}/^{144}\text{Nd}$ ($R^2 = 0.1043$) diagram, this contradicts the hypothesis of the presence of two-component mixing. The approximation of the ^{147}Sm – ^{143}Nd whole-rock isotopic data obtained for dunite, gabbro, clinopyroxenite, and wehrlite was characterized by an isochronous dependence (MSWD = 0.17) corresponding to the age of 503 ± 15 Ma. Following a similar procedure applied to ^{147}Sm – ^{143}Nd data (whole-rock and mineral fraction analyses (7 points)), the $^{147}\text{Sm}/^{144}\text{Nd}$ – $^{143}\text{Nd}/^{144}\text{Nd}$ evolutionary diagram was constructed. It allows calculating the primary ratio $(^{143}\text{Nd}/^{144}\text{Nd})_0 = 0.512289 \pm 0.000027$ and age (MSWD = 2.4) 514 ± 17 Ma (95% confidence level), which corresponds to the first half of the Cambrian according to the modern International Chronostratigraphic Chart (ver. 2022/02). This age coincides within the limits of the measurement errors with the whole-rock age, as well as with the ^{147}Sm – ^{143}Nd age data on three samples of clinopyroxenites and extracted clinopyroxenes (499 ± 13 Ma) presented in ref. [6]. In terms of the CHUR model, the

calculated primary ratio ($^{143}\text{Nd}/^{144}\text{Nd}$)₀ = 0.512289 ± 0.000027) corresponds to ε_{Nd} = +6.1 that is characteristic of the depleted source of the studied rocks.

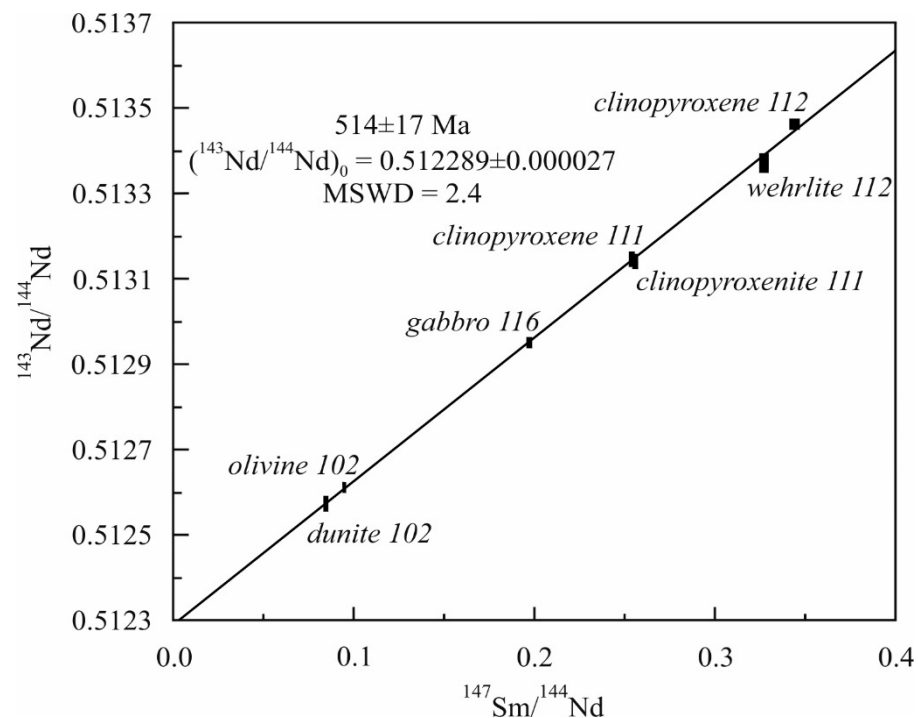


Figure 4. Nicolaysen evolutionary diagram for the rocks and minerals of the Kluchevskoy massif.

4.3. Results of Studying Inclusions in Zircon

The isotopic ages obtained by two methods: the ^{147}Sm – ^{143}Nd isochronous method for whole-rock samples and monofractions of rock-forming minerals and the U–Pb method, differing by about 70 Ma. In this regard, it became necessary to conduct additional research to explain the reasons for the differences revealed. For this purpose, we studied the compositions of silicate inclusions in zircon grains. The fact that the inclusions were captured by zircon during its crystallization allowed us to consider them as syngenetic to zircon. Due to this fact, they carry information about the conditions of their joint crystallization. Mineral inclusions appropriate for assessing the crystallization conditions of dated zircon grains were found only in zircons from gabbro (Figure 2d). The analytical data given in Table 4 show that they are represented by typical metamorphic minerals: amphibole, albite, and zoisite (or clinozoisite), similar in composition to the rock-forming minerals of the studied sample of gabbro. At the same time, the composition of these minerals both in the rock and in inclusions varies noticeably. One of the studied zircon grains contains inclusions of albite and edenite (analyses 7 and 5, Figure 2d; Table 4). This mineral association corresponds to the moderate-pressure epidote–amphibolite facies of metamorphism. This is confirmed by the evaluation of the P – T parameters of the crystallization of this pair of minerals using well-known geothermometers and geobarometers [27–33]. The calculations following the different geothermometers and geobarometers showed that the joint crystallization of plagioclase and amphibole of this composition corresponds to crystallization in the P – T range of 418–567 °C and 2.5–4 kbar that corresponds to upper greenschist and the lower epidote–amphibolite facies metamorphism. Another studied zircon grain contains inclusions of minerals of the low- T greenschist paragenesis: albite and ferruginous tremolite (analyses 8, 9, and 6). The composition of minerals from inclusions in this zircon grain indicates its crystallization at comparable temperatures of 411–602 °C and a significantly lower pressure of less than 1 kbar.

Table 4. Chemical composition of mineral inclusions in zircons from the gabbro Kluchevskoy massif (wt%).

No	1	2	3	4	5	6	7	8	9	10	11
SiO ₂	40.42	39.65	52.76	52.79	49.20	55.51	67.98	67.65	67.76	67.19	68.28
TiO ₂	0.04	0.03	0.44	0.32	0.18	0.14	-	-	-	-	0.01
Al ₂ O ₃	32.31	32.76	3.77	4.03	7.52	1.18	20.45	20.53	20.53	21.07	20.42
Cr ₂ O ₃	-	-	0.17	0.14	-	0.01	-	-	-	-	-
Fe ₂ O ₃	0.22	0.46	-	-	-	-	-	-	-	-	-
FeO	-	-	8.61	7.56	10.34	9.57	-	-	-	-	-
MnO	0.01	0.16	0.24	0.21	0.15	0.24	0.01	0.02	0.01	0.05	-
MgO	0.02	0.05	17.87	18.06	15.29	17.71	-	-	-	-	-
CaO	24.08	24.22	11.43	11.88	11.62	11.68	0.62	0.73	0.83	1.18	0.25
Na ₂ O	0.60	0.14	1.24	1.04	1.68	0.42	11.39	11.49	11.66	11.28	11.69
K ₂ O	0.01	0.01	0.05	0.06	0.15	0.03	0.07	0.08	0.05	0.05	0.05
Total	97.71	97.47	96.60	96.10	96.12	96.49	100.51	100.51	100.84	100.82	100.71
Coefficients of crystal chemical formulas											
Si	3.06	3.01	7.94	7.96	7.45	8.46	2.96	2.94	2.93	2.92	2.97
Ti	-	-	0.05	0.04	0.02	0.02	-	-	-	-	-
Al	2.88	2.94	0.67	0.71	1.34	0.21	1.05	1.05	1.05	1.08	1.04
Cr	-	-	0.02	0.02	-	-	-	-	-	-	-
Fe ³⁺	0.02	0.03	-	-	-	-	-	-	-	-	-
Fe ²⁺	-	-	1.08	0.95	1.31	1.22	-	-	-	-	-
Mn	-	0.01	0.03	0.03	0.02	0.03	-	-	-	-	-
Mg	-	0.01	4.00	4.06	3.45	4.02	-	-	-	-	-
Ca	1.95	1.98	1.84	1.92	1.89	1.91	0.03	0.03	0.04	0.05	0.01
Na	0.09	0.02	0.36	0.30	0.49	0.12	0.96	0.97	0.98	0.95	0.98
K	-	-	0.01	0.01	0.03	0.01	-	0.01	-	-	-
Total	8.00	8.00	16.00	16.00	16.00	16.00	5.00	5.00	5.00	5.00	5.00

Note. 1–2—grains of the epidote mineral group (zoisite or clinocoisite); 3–6—amphiboles (3, 4, and 6—ferruginous tremolites, 5—edenite); 7–11—albites.

5. Discussion

According to the obtained data, silicate inclusions occurring in dated zircon grains are represented by typical metamorphic minerals, which indicate the metamorphic origin of the host zircon. This means that the age range of 456–441 Ma of dated zircon grains of the predominant population records a large, in all likelihood, the most significant stage of metamorphism manifested in all rocks of the ophiolite association of the Kluchevskoy massif. The *P–T* conditions of zircon crystallization established on the basis of the analysis of the composition of minerals of inclusions show that the zircon crystallization occurred during metamorphism of gabbro under the lower epidote–amphibolite and upper greenschist facies under decompression conditions, i.e., during the uplift from the deep horizons (8–13 km) to the crustal subsurface level.

Another stage of metamorphism of the rocks of Kluchevskoy massif was detected via dating of the U-rich zircon composing the rims of zircon grains (Figure 2; Table 2). The proportion of such zircon is usually insignificant except for the mantle dunite of sample 11-1, where this zircon variety dominates. This indicates a much lower degree of rock transformations at this stage of metamorphism. The crystallization of U-rich zircon rims at 318.1–277.4 Ma (the second half of the Carboniferous and the beginning of the Permian) coincides with the time of collision and orogeny in the Ural mobile belt and it was apparently due to the thermal effect of numerous granitoid intrusions emplaced at that time. A rather wide age range (more than 40 Ma) that recorded this stage of rock transformations can be most likely explained not by measurement errors, but by the duration (and repeated continuation) of the collision process in the Urals.

Thus, the data obtained indicate that while estimating the formation time of the rocks of the Kluchevskoy ophiolite massif, the ancient ¹⁴⁷Sm–¹⁴³Nd age data (499 ± 13 and 514 ± 17 Ma) of rocks of the layered complex are crucial, but not the results of the U–Pb zircon dating. Most likely these age values can be considered as the time of formation of the layered dunite–wehrlite–clinopyroxenite–gabbro complex in the oceanic crust. At the same time, the obtained ¹⁴⁷Sm–¹⁴³Nd age data may also be partially rejuvenated. Therefore, it

should be considered apparently only as the upper age boundary of the formation of the studied ophiolite association.

When deciphering the geological meaning of U–Pb ages 456–441 Ma, an assessment of the P–T conditions of metamorphism of this stage is important. According to the data obtained, metamorphism occurred during the movement of rocks from depths of 8–13 km, i.e., from the lower part of the oceanic crust to its near-surface horizons, which exactly corresponds to the conditions of the processes of obduction. This is consistent with the existing understanding of the history of the development of the Ural mobile belt. To date, it has been reliably established that for a period of 456–441 Ma ago, the Urals was the site of a collision of the oceanic plate with the margin of the newly formed East Ural continent, as a result of which the Late Ordovician–Silurian Island arc was formed (refs. [34,35], etc.).

Finally, it should be noted that a lot of Late Ordovician–Early Silurian age data have been obtained for the rocks of the ophiolite complexes of the Urals and they have been often interpreted as the time of their formation (refs. [3,5,7], etc.). At the same time, any substantiation of the fact that the obtained age data recorded the time of formation of rocks and not a later event has not been previously stated. We suggest that the dates of zircons from the rocks of the Kluchevskoy ophiolite massif within this age range marked the time of their metamorphic transformations. In this regard, until more reliable data are obtained suggesting that the Late Ordovician–Silurian isotopic ages of rocks from different parts of the Urals reflect the formation time of ophiolites, the presence of plutonic rocks of the ophiolite association of this age cannot be considered proven.

6. Conclusions

The age data obtained for the rocks of the Kluchevskoy ophiolite massif by two methods of isotopic geochronology differed greatly. The ^{147}Sm – ^{143}Nd dating of dunite, wehrlite, clinopyroxenite, and gabbro from the layered part of the ophiolite association yielded an age of 514 ± 17 Ma. At the same time, the U–Pb (SHRIMP-II) age data of zircons from rocks of both mantle and crustal (layered) parts of the ophiolite association of the studied massif varied from 441 to 456 Ma. The analysis of the composition of silicate inclusions in dated zircon grains showed that the much younger U–Pb ages of this zircon can be explained by its metamorphic genesis. The largest portion of this zircon crystallized during the metamorphism of rocks under the lower epidote–amphibolite and upper greenschist facies shows metamorphism with decreasing pressure during the uplift of rocks from depths of 8–13 km into the subsurface crustal level. The crystallization of a relatively small amount of zircon (U-rich rims of grains), apparently, was associated with the transformation of rocks under the thermal influence of orogenic granitoid intrusions. Thus, the more ancient ^{147}Sm – ^{143}Nd age of 514 Ma should be assumed as the formation time of rocks (or its upper age boundary).

The data obtained indicate the need to interpret the results of isotopic dating of ophiolites with great care. The geological conclusions based on the obtained isotopic ages in each case need careful justification.

Author Contributions: Conceptualization, V.N.S. and K.S.I.; resources, V.N.S. and K.S.I.; formal analysis, Y.L.R. and Y.V.E.; methodology, V.N.S.; visualization, Y.V.E.; writing—review and editing, V.N.S., K.S.I. and Y.L.R. All authors have read and agreed to the published version of the manuscript.

Funding: The research was carried out at the expense of the grant of the Russian Science Foundation No. 22-17-00027.

Acknowledgments: We are grateful to N.V. Rodionov, an employee of the VSEGEI Center of Isotopic Research, for the U–Pb isotopic analyses of zircons, as well as to the staff of the Institute of Geology and Geochemistry of the Ural Branch of the Russian Academy of Sciences, V.V. Khiller for microprobe study of the composition of silicate inclusions in zircon grains, N.P. Gorbunova, V.P. Vlasov, G.S. Neupokoeva for X-ray fluorescence analysis of rocks and determination of the contents of the major petrogenic elements and D.V. Kiseleva and N.V. Cherednichenko for the ICP-MS trace elemental analysis.

Conflicts of Interest: The authors declare no conflict of interest. The funders had no role in the design of the study; in the collection, analyses, or interpretation of data; in the writing of the manuscript, or in the decision to publish the results.

References

1. Gurskaya, L.I.; Smelova, L.V. PGE mineral formation and the structure of the Syum-Keu massif (Polar Urals). *Geol. Ore Deposit.* **2003**, *45*, 309–325.
2. Khain, E.V.; Fedotova, A.A.; Salnikova, E.V.; Kotov, A.V.; Kovach, V.P.; Yakovleva, S.Z.; Burgath, K.P.; Schaefer, F.; Remizov, D.N. U–Pb age of plagiogranites from the ophiolite association in the Voikar–Synya Massif, Polar Urals. *Dokl. Earth Sci.* **2008**, *419*, 392–396. [[CrossRef](#)]
3. Krasnobaev, A.A.; Rusin, A.I.; Busharina, S.V.; Rodionov, N.V. Zirconology of ultramafic rocks from the Vostochno-Tagilsky massif (Middle Urals). *Dokl. Earth Sci.* **2014**, *455*, 441–445. [[CrossRef](#)]
4. Krasnobaev, A.A.; Rusin, A.I.; Busharina, S.V.; Valizer, P.M.; Anfilogov, V.N.; Medvedeva, E.V.; Sergeev, S.A. Zirconology of ultrabasic rocks of the Karabashsky massif (Southern Urals). *Dokl. Earth Sci.* **2016**, *469*, 647–679. [[CrossRef](#)]
5. Petrov, G.A.; Ronkin, Y.L.; Maslov, A.V.; Lepikhina, O.P. Vendian and Silurian ophiolite-formation stages on the Eastern slope of the Middle Urals. *Dokl. Earth Sci.* **2010**, *432*, 570–576. [[CrossRef](#)]
6. Popov, V.S.; Kremenetsky, A.A.; Belyatsky, B.V. Pre-Ordovician Sm–Nd isotopic age of ultramafic rocks in the ophiolite of the Urals: Specified data. In *Structural-Substantial Complexes and the Problems of Geodynamics of the Precambrian Phanerozoic Orogens*; Institute of Geology and Geochemistry UB RAS: Yekaterinburg, Russia, 2008; pp. 100–103. (In Russian)
7. Remizov, D.N.; Petrov, S.Y.; Kos'yanov, A.O.; Nosikov, M.V.; Sergeev, S.A.; Grigoriev, S.L. New age dating of gabbroids of the Kershov complex (Polar Urals). *Dokl. Earth Sci.* **2010**, *434*, 1235–1239. [[CrossRef](#)]
8. Savelieva, G.N.; Batanova, V.G.; Sobolev, A.V.; Belousov, I.A.; Berezhnaya, N.A.; Presnyakov, S.L.; Skublov, S.G. Polychronous formation of mantle complexes in ophiolites. *Geotectonics* **2013**, *47*, 167–179. [[CrossRef](#)]
9. Savelieva, G.N.; Suslov, P.V.; Larionov, A.N. Vendian tectono-magmatic events in mantle ophiolitic complexes of the Polar Urals: U–Pb dating of zircon from chromitites. *Geotectonics* **2007**, *41*, 105–113. [[CrossRef](#)]
10. Smirnov, V.N.; Ivanov, K.S. The first zircon U–Pb dating (SHRIMP-II) for the Silurian ophiolites in the Urals. *Dokl. Earth Sci.* **2010**, *430*, 15–18. [[CrossRef](#)]
11. Anfilogov, V.N.; Krasnobaev, A.A.; Valizer, P.M. The age of ultramafic rocks of the main Ural Fault. *Dokl. Earth Sci.* **2018**, *482*, 1249–1251. [[CrossRef](#)]
12. Ronkin, Y.L.; Karaseva, T.V.; Maslov, A.V. The First ^{147}Sm – ^{143}Nd Data on Rocks from the 6925.2- to 8250-m Interval of the SG-7 Superdeep Borehole (West Siberian Oil-and-Gas Province). *Dokl. Earth Sci.* **2021**, *496*, 130–134. [[CrossRef](#)]
13. Larionov, A.N.; Andreichev, V.A.; Gee, D.G. The Vendian alkaline igneous suite of northern Timan: Ion microprobe U–Pb zircon ages of gabbros and syenite. The Neoproterozoic Timanide Orogen of Eastern Baltica. *Geol. Soc.* **2004**, *30*, 69–74. [[CrossRef](#)]
14. Williams, I.S. U–Th–Pb geochronology by ion microprobe. *Rev. Econ. Geol.* **1998**, *7*, 1–35.
15. Black, L.P.; Kamo, S.L.; Allen, C.M.; Aleinikoff, J.N.; Davis, D.W.; Korsch, R.J.; Foudoulis, C. TEMORA 1: A new zircon standard for Phanerozoic U–Pb geochronology. *Chem. Geol.* **2003**, *200*, 155–170. [[CrossRef](#)]
16. Black, L.P.; Kamo, S.L.; Allen, C.M.; Davis, D.W.; Aleinikoff, J.N.; Valley, J.W.; Mundil, R.; Campbell, I.H.; Korsch, R.J.; Williams, I.S.; et al. Improved $^{206}\text{Pb}/^{238}\text{U}$ microprobe geochronology by the monitoring of a trace-element-related matrix effect; SHRIMP, ID–TIMS, ELA–ICP–MS and oxygen isotope documentation for a series of zircon standards. *Chem. Geol.* **2004**, *205*, 115–140. [[CrossRef](#)]
17. Wiedenbeck, M.; Hanchar, J.M.; William, H.; Peck, W.H.; Sylvester, P.; Valley, J.; Whitehouse, M.; Kronz, A.; Morishita, Y.; Nasdala, L.; et al. Further characterization of the 91500 zircon crystal. *Geostand. Geoanal. Res.* **2004**, *28*, 9–39. [[CrossRef](#)]
18. Wiedenbeck, M.; Allé, P.; Corfu, F.; Griffin, W.L.; Meier, M.; Oberli, F.; von Quadt, A.; Roddick, J.C.; Spiegel, W. Three Natural Zircon Standards for U–Th–Pb, Lu–Hf, Trace Element and REE Analyses. *Geostand. Newslett.* **1995**, *19*, 1–23. [[CrossRef](#)]
19. Smirnov, V.N.; Fershtater, G.B.; Ivanov, K.S. Scheme of tectonomagmatic zoning of the eastern slope of Middle Urals. *Lithosphere* **2003**, *2*, 40–56. (In Russian)
20. Ivanov, K.S.; Puchkov, V.N.; Fyodorov, Y.N.; Erokhin, Y.V.; Pogromskaya, O.E. Tectonics of the Urals and adjacent part of the West-Siberian platform basement: Main features of geology and development. *J. Asian Earth Sci.* **2013**, *72*, 12–24. [[CrossRef](#)]
21. Smirnov, V.N.; Ivanov, K.S. Structural connections between the Urals and West Siberia: The common stage on the boundary of Permian and Triassic periods. *Dokl. Earth Sci.* **2019**, *488*, 294–297. [[CrossRef](#)]
22. Coleman, R.G. *Ophiolites: Ancient Oceanic Lithosphere?* Springer: Berlin/Heidelberg, Germany, 1997; p. 229.
23. Scherbakov, S.A. *Plastic Deformations of Ultramafics from the Urals Ophiolite Association*; Nauka Publishing House: Moscow, Russia, 1990; p. 117. (In Russian)
24. Simonov, V.A.; Smirnov, V.N.; Ivanov, K.S.; Kovyazin, S.V. Melt inclusions in chrome spinelids of the stratified part of the Klyuchevskoy gabbro-hyperbasite massif. *Lithosphere* **2008**, *2*, 101–115. (In Russian)
25. Zaccarini, F.; Pushkarev, E.; Garuti, G. Platinum-group element mineralogy and geochemistry of the Kluchevskoy ophiolite complex, central Urals (Russia). *Ore Geol. Rev.* **2008**, *33*, 20–30. [[CrossRef](#)]
26. Perevozchikov, B.V. (Ed.) *Register Shows of Chromite Occurrences in Alpine-Type Peridotites of Urals*; Star Publishing House: Perm, Russia, 2000; p. 474. (In Russian)

27. Hammarstrom, J.M.; Zen, E.-A. Aluminum in hornblende: An empirical igneous geobarometer. *Amer. Miner.* **1986**, *76*, 1297–1313.
28. Holland, T.; Blundy, J. Non-ideal interactions in calcic amphiboles and their bearing on amphibole-plagioclase thermometry. *Contrib. Miner. Petrol.* **1994**, *116*, 433–447. [[CrossRef](#)]
29. Jaques, A.L.; Blake, D.H.; Donchak, P.J.T. Regional metamorphism in the Selwin Range area, north-west Queensland. *J. Austral. Geol. Geophys.* **1982**, *7*, 181–196.
30. Molina, J.F.; Moreno, J.A.; Castro, A.; Rodrigues, C.; Fershtater, G.B. Calcic amphibole thermobarometry in metamorphic and igneous rocks: New calibrations based on plagioclase/amphibole Al-Si partitioning and amphibole/liquid Mg partitioning. *Lithos* **2015**, *232*, 286–305. [[CrossRef](#)]
31. Otten, M.T. Origin of brown hornblende in the Artfjallet gabbro and dolerites. *Contrib. Miner. Petrol.* **1984**, *86*, 189–199. [[CrossRef](#)]
32. Schmidt, M.W. Amphibole composition in tonalites as a function of pressure: An experimental calibration of the Al-in-hornblende barometer. *Contrib. Miner. Petrol.* **1992**, *110*, 304–310. [[CrossRef](#)]
33. Spear, F.S. Amphibole-plagioclase equilibria: An empirical model for the relation albite+tremolite = edenite+quartz. *Contrib. Miner. Petrol.* **1981**, *77*, 355–364. [[CrossRef](#)]
34. Dymkin, A.M.; Ivanov, K.S.; Ivanov, S.N.; Krasnobaev, A.A.; Poltavetz, Y.A.; Pumpyansky, A.I.; Puchkov, V.N.; Rusin, A.I.; Samarkin, G.I.; Semenov, I.V. *Formation of the Earth Crust of the Urals*; Nauka Publishing House: Moscow, Russia, 1986; p. 248. (In Russian)
35. Ivanov, K.S. *The Main Features of the Geological History (1.6–0.2 Ga) and the Structure of the Urals*; Institute of Geology and Geochemistry UB RAS: Yekaterinburg, Russia, 1998; p. 252. (In Russian)